IEEE Access
Multidisciplinary | Rapid Review | Open Access Journal

Received 18 September 2023, accepted 3 October 2023, date of publication 5 October 2023, date of current version 11 October 2023.

Digital Object Identifier 10.1109/ACCESS.2023.3322368

RESEARCH ARTICLE

An Integral Formulation for Rectangular Wires in a 3D Magneto-Quasi-Static Field

PASQUALE CAMBARERI[1], LUCA DI RIENZO[1], (Senior Member, IEEE), MASSIMO BECHIS[2], AND CARLO DE FALCO[3]

[1]Dipartimento di Elettronica, Informazione e Bioingegneria, Politecnico di Milano, 20133 Milan, Italy
[2]Prysmian S.p.A., 20126 Milan, Italy
[3]MOX, Dipartimento di Matematica, Politecnico di Milano, 20133 Milan, Italy

Corresponding author: Luca Di Rienzo (luca.dirienzo@polimi.it)

The work of Carlo de Falco was supported in part by the Italian Research Center on High-Performance Computing, Big Data and Quantum Computing (ICSC), European Union-Next Generation EU.

ABSTRACT This paper proposes an integral formulation for calculating the magnetic and ohmic losses in rectangular wires immersed in an external 3D magneto-quasi-static field. The formulation is based on some simplifying assumptions that allow to employ a collocation method with constant elements for the discretization, reducing the computational burden. Even if the assumptions introduce an approximation, for the application at hand the numerical tests have shown that the accuracy is still acceptable. Moreover, the computational time is drastically reduced with respect to other approaches based on the finite element method.

INDEX TERMS Integral equation formulations, rectangular wires, collocation method, eddy currents.

I. INTRODUCTION

Rectangular wires are widely utilized in electrical systems, e.g. for coils in transformers and rotating machines [1], [2], or for mechanical armours in submarine power cables [3]. Depending on the application, such wires can be purely conductive or both conductive and ferromagnetic. An accurate numerical simulation of the electromagnetic behaviour of these wires is required to calculate the power losses due to induced eddy currents and to magnetic hysteresis [4].

Traditional formulations based on the finite element method (FEM) suffer from a high number of degrees of freedom, that leads to a large demand of memory and computation time. To face these limitations integral equation formulations come in useful. By reducing the computational geometry solely to the wires themselves, without the need of discretizing the remaining volume as in FEM, they significantly reduce the computational burden by requiring less degrees of freedom.

This paper presents such an integral equation formulation for the calculation of eddy currents and hysteresis losses in rectangular wires. The formulation is based on simplifying assumptions that limit the accuracy to a level still acceptable for some applications, and allows for an efficient solution of the problem.

Section II presents the magnetostatic integral formulation for a single wire, which is then discretized in section III. Section IV addresses a specific technical aspect of the presented formulation, which is particularly delicate. Section V presents the validation of the magnetostatic formulation derived in the previous sections. Section VI extends the presented formulation to the time-harmonic regime and section VII presents its numerical validation. Eventually, section VIII discusses the application of the presented method to the case of armoured AC submarine cables.

II. MAGNETOSTATIC INTEGRAL FORMULATION FOR A SINGLE WIRE

The present formulation is derived starting from the work developed in [7], [4], [5] and [6], which focused on wires of circular cross-section, and it was based, in turn, on the work in [8] and [9]. In the presence of a wire with relative magnetic permeability μ_r, the three-dimensional space can be partitioned into Ω_M, which is the domain occupied by

The associate editor coordinating the review of this manuscript and approving it for publication was Fulvio Schettino.

the wire, and Ω_0, which is the remaining part, namely air. Under the influence of an external, known magnetostatic flux density $\mathbf{B}_0$ the wire is magnetized with magnetization $\mathbf{M}$. The field, $\mathbf{B}_M$, due to such a magnetization is retrieved from the well-known Biot-Savart formula [10]

$$\mathbf{B}_M = \frac{\mu_0}{4\pi}\int_{\Omega_M} \left(\nabla\times\mathbf{M}\right)(\mathbf{x}')\times\frac{\mathbf{x}-\mathbf{x}'}{|\mathbf{x}-\mathbf{x}'|^3}\,d^3x' + \frac{\mu_0}{4\pi}\int_{\partial\Omega_M}\left(\mathbf{n}\times[\![\mathbf{M}]\!]\right)(\mathbf{x}')\times\frac{\mathbf{x}-\mathbf{x}'}{|\mathbf{x}-\mathbf{x}'|^3}\,d^2x', \quad (1)$$

where $[\![\mathbf{M}]\!]$ is the jump discontinuity of the magnetization across boundary $\partial\Omega_M$ caused by the different permeabilities of wire, $\mu_0\mu_r$, and air, μ_0 [5]. Being $\mathbf{B} = \mathbf{B}_0 + \mathbf{B}_M$ the total magnetic flux density in the wire, the relation between magnetization and magnetic flux density is given by

$$\begin{aligned}\mathbf{M}(\mathbf{x}) &= \mathbf{B}(\mathbf{x})/\mu_0 - \mathbf{H}(\mathbf{x})\\ &= \mathbf{B}(\mathbf{x})/\mu_0 - \mathbf{B}(\mathbf{x})/(\mu_0\mu_r)\\ &= \frac{\kappa}{\mu_0}\left(\mathbf{B}_0(\mathbf{x})+\mathbf{B}_M(\mathbf{x})\right) \qquad \mathbf{x}\in\Omega_M,\end{aligned} \quad (2)$$

with $\kappa = 1 - 1/\mu_r$.

III. DISCRETIZATION

The magnetostatic formulation developed in [4], [5], [6], and [7] considered the magnetization to be uniform over the round wire cross-section. It can be shown analytically that this is indeed the case for infinitely long, straight round wires, provided that the external field $\mathbf{B}_0$ is uniform, [4], [10], [11]. In particular, the wire domain was discretized into n cylinders and a piecewise constant approximation for the magnetization was adopted,

$$\mathbf{M}(\mathbf{x}) = \sum_{i=1}^{n}\mathbf{M}^{(i)}\mathbb{1}^{(i)}(\mathbf{x}), \quad (3)$$

where $\mathbb{1}^{(i)}$ was the indicator function of the i-th cylinder and $\mathbf{M}^{(i)}$ was the magnetization in that cylinder. The same approach will be followed here for rectangular wires, however it should be noted that the magnetization is not uniform in this case: the proposed method then is characterized by an intrinsic modelling error that will be discussed later in the paper.

In order to apply the collocation method with constant elements the wire is discretized into rectangular cuboids with thickness d, width w and height h, as shown by Fig. 1. The geometric centre of each cuboid will be indicated as $\mathbf{x}^{(i)} \in \Omega_M$, being $i \in \mathbb{N}$ an index to identify the cuboid. Point $\mathbf{x}^{(i)}$ is the collocation point where the supposed uniform magnetization is considered. In each collocation point a local frame of reference $\mathbf{e}_1^{(i)}$, $\mathbf{e}_2^{(i)}$ and $\mathbf{e}_3^{(i)}$ is placed. The face of each cuboid perpendicular to the local direction $\mathbf{e}_3^{(i)}$ is referred to as the cross-section, S, and its area is given by $|S| = \mathcal{S} = w\cdot d$.

For the later extension of the formulation to the AC case, section VI, it is convenient to formulate the discretized

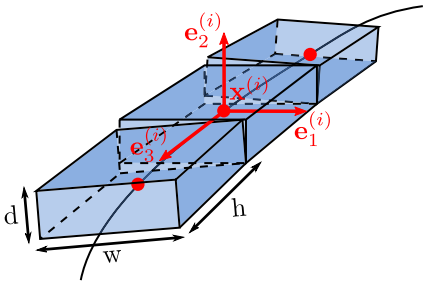

FIGURE 1. Rectangular wire discretization. Collocation point $\mathbf{x}_i$ is the origin for the local coordinate system $\mathbf{e}_1^{(i)}$, $\mathbf{e}_2^{(i)}$ and $\mathbf{e}_3^{(i)}$.

problem in terms of the magnetic moment per unit length,

$$\mathbf{m} = \int_S \mathbf{M}(\mathbf{x}')d^2x'. \quad (4)$$

Under the assumption of uniformity and being $\mathbf{M}^{(i)} = \mathbf{M}(\mathbf{x}^{(i)})$, it follows that

$$\mathbf{m}^{(i)} = \mathbf{M}^{(i)}\mathcal{S}. \quad (5)$$

The reason for this choice, that was already made in [4], [5], and [6], will be clear later in the paper, when the formulation will be extended to the time-harmonic case.

The next step is the discretization of (2). Applying (2) in $\mathbf{x}^{(i)}$, multiplying by $\mathcal{S}$ and then using (5) yields

$$\mathbf{m}^{(i)} = \frac{\kappa\mathcal{S}}{\mu_0}\left(\mathbf{B}_0^{(i)} + \mathbf{B}_M^{(i)}\right), \quad (6)$$

where $\mathbf{B}_0^{(i)} = \mathbf{B}_0(\mathbf{x}^{(i)})$ and $\mathbf{B}_M^{(i)} = \mathbf{B}_M(\mathbf{x}^{(i)})$. Term $\mathbf{B}_M^{(i)}$ is calculated with equation (1), where the first integral involving $\nabla\times\mathbf{M}$ vanishes because of the uniform magnetization in each cuboid. As for the second integral, we note first of all that [5]

$$[\![\mathbf{M}]\!] = \mathbf{M}_0 - \mathbf{M}, \quad (7)$$

being $\mathbf{M}_0$ the magnetization in Ω_0. Knowing that there is no magnetization in air, i.e. $\mathbf{M}_0 = 0$, we obtain, using (5),

$$[\![\mathbf{M}]\!](\mathbf{x}^{(i)}) = -\frac{\mathbf{m}^{(i)}}{\mathcal{S}}. \quad (8)$$

Indicating with $\Omega_M^{(i)}$ the domain of each cuboid and with $\partial\Omega_M^{(i)}$ its boundary, the final discretized form of (1) is

$$\mathbf{B}_M^{(i)} = \sum_{j=1}^{n} -\frac{\mu_0}{4\pi}\int_{\partial\Omega_M^{(j)}}\left(\mathbf{n}(\mathbf{x}')\times\frac{\mathbf{m}^{(j)}}{\mathcal{S}}\right)\times\frac{\mathbf{x}^{(i)}-\mathbf{x}'}{|\mathbf{x}^{(i)}-\mathbf{x}'|^3}d^2x', \quad (9)$$

where it is assumed that the wire is discretized into n cuboids. Vector $\mathbf{m}^{(j)}$ can be written in its local coordinate system as

$$\mathbf{m}^{(j)} = \sum_{k=1}^{3} m_k^{(j)}\mathbf{e}_k^{(j)}. \quad (10)$$

Hence, substituting (10) into (9), and after defining

$$\mathbf{a}_k^{(i,j)} = -\frac{\mu_0}{4\pi}\int_{\partial\Omega_M^{(j)}} \left(\mathbf{n}(\mathbf{x}') \times \frac{\mathbf{e}_k^{(j)}}{\mathcal{S}}\right) \times \frac{\mathbf{x}^{(i)} - \mathbf{x}'}{|\mathbf{x}^{(i)} - \mathbf{x}'|^3} d^2x', \tag{11}$$

equation (9) becomes

$$\mathbf{B}_M^{(i)} = \sum_{j=1}^{n}\sum_{k=1}^{3} \mathbf{a}_k^{(i,j)} m_k^{(j)}. \tag{12}$$

This last equation can be written in a more convenient manner as

$$\mathbf{B}_M^{(i)} = \sum_{j=1}^{n} A^{(i,j)}\mathbf{m}^{(j)}, \tag{13}$$

where $A^{(i,j)} \in \mathbb{R}^{3\times 3}$ is given by

$$A^{(i,j)} = \left[\mathbf{a}_1^{(i,j)}\ \mathbf{a}_2^{(i,j)}\ \mathbf{a}_3^{(i,j)}\right]. \tag{14}$$

The substitution of (13) into (6), and the application of the resulting relationship to each collocation point, yields the linear system of equations

$$\left(\mathrm{I} - \frac{\kappa\mathcal{S}}{\mu_0}A\right)\mathbf{u} = \frac{\kappa\mathcal{S}}{\mu_0}\mathbf{b}, \tag{15}$$

where $I \in \mathbb{R}^{3n\times 3n}$ is the identity, whereas

$$A = \begin{bmatrix} A^{(1,1)} & \dots & A^{(1,n)} \\ \vdots & \ddots & \vdots \\ A^{(n,1)} & \dots & A^{(n,n)} \end{bmatrix}, \tag{16}$$

and

$$\mathbf{u} = \begin{bmatrix} \mathbf{m}^{(1)} \\ \vdots \\ \mathbf{m}^{(n)} \end{bmatrix}, \qquad \mathbf{b} = \begin{bmatrix} \mathbf{B}_0^{(1)} \\ \vdots \\ \mathbf{B}_0^{(n)} \end{bmatrix}. \tag{17}$$

IV. SELF-ELEMENT CALCULATION

Sub-matrices $A^{(i,i)}$ in (16) are called "self-elements," and in their calculation the assumption of uniform magnetization is too restrictive so that (11) cannot be used. The self-element calculation should then be addressed by applying a unitary magnetic moment in point $\mathbf{x}^{(i)}$ of Fig. 1 and by calculating the resulting magnetic flux density in the corresponding cuboid. However, this section illustrates an alternative approach that reduces the problem to only two dimensions, reducing the computational complexity.

To tackle the problem, let us focus on the simplified configuration of a straight and infinitely long wire, shown by Fig. 2. Referring to this case study is not restrictive, as the final goal is to calculate the self-element of a single cuboid, which is independent from the position of the remaining ones. Note also that in this case there is a common local reference frame to all collocation points, namely $\mathbf{e}_1$, $\mathbf{e}_2$ and $\mathbf{e}_3$. If the wire is infinite then the number of collocation points is infinite as well, hence equation (13) is rewritten as

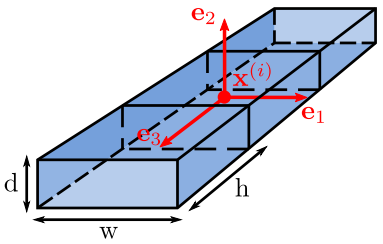

FIGURE 2. Infinite straight wire discretization. In this case there is a common reference frame $\mathbf{e}_1$, $\mathbf{e}_2$ and $\mathbf{e}_3$ to all collocation points.

$$\mathbf{B}_M^{(i)} = \sum_{j\in\mathbb{Z}} A^{(i,j)}\mathbf{m}^{(j)} \qquad \forall i \in \mathbb{Z}. \tag{18}$$

Now let us introduce a new assumption, i.e. that the externally imposed magnetic field is uniform and directed along one of the canonical directions $\mathbf{e}_k$. More precisely, we impose that

$$\mathbf{B}_0^{(i)} = \mu_0 H_0 \mathbf{e}_k \qquad \forall i \in \mathbb{Z}, \tag{19}$$

where H_0 is an arbitrary magnetic field and can be trivially set equal to 1 A/m. Again this is not restrictive, as the self-element is independent from the external field. This assumption implies that the magnetization is the same along the entire wire, therefore $\mathbf{m}^{(j)} = \mathbf{m}^{(i)}$, $\forall i, j \in \mathbb{Z}$. Thus, taking $i = 0$ as the index of the reference collocation point, we can write

$$\mathbf{B}_M^{(0)} = \left(A^{(0,0)} + \sum_{j\in\mathbb{Z}\setminus\{0\}} A^{(0,j)}\right)\mathbf{m} = (A_s + A_e)\,\mathbf{m}, \tag{20}$$

where $\mathbf{m}^{(j)} = \mathbf{m}$, $\forall j \in \mathbb{Z}$, $A_s = A^{(0,0)}$ is the self-element and

$$A_e = \sum_{j\in\mathbb{Z}\setminus\{0\}} A^{(0,j)} \tag{21}$$

is the total contribution of the other elements.

The remaining part of the discussion relies on two fundamental properties of A_s and A_e. First of all, A_e must be finite, which is not automatically guaranteed as it is obtained from an infinite series. Second, both A_s and A_e must be diagonal matrices. In order to keep the current discussion simple and linear, the proof of these important properties has been postponed to Appendix A.

Using (19) and (20) system (15) for the infinite straight wire becomes

$$\left(\mathrm{I} - \frac{\kappa\mathcal{S}}{\mu_0}(A_s + A_e)\right)\mathbf{m} = \kappa\mathcal{S}\begin{bmatrix} H_0 \\ H_0 \\ H_0 \end{bmatrix}. \tag{22}$$

Let now m_k be the k-th component of $\mathbf{m}$, and α_{kk} and β_{kk} be the non-zero diagonal coefficients of A_s and A_e, respectively. Note that β_{kk} can be obtained from (21), (14) and (11). The

above linear system written on the k-th component, then, gives

$$\left(1 - \frac{\kappa\mathcal{S}}{\mu_0}\left(\alpha_{kk} + \beta_{kk}\right)\right) m_k = \kappa\mathcal{S}H_0. \tag{23}$$

An infinite straight wire geometry in a uniform magnetic field is a two-dimensional problem. Since the magnetization does not change along the axial direction, $\mathbf{e}_3$: the problem can be studied on the wire cross-section. The value of the m_k in (23) then can be obtained by solving a two-dimensional boundary value problem using, for example, finite elements. Once m_k is known, the self-element coefficients α_{kk} can be calculated as

$$\alpha_{kk} = \frac{\mu_0}{\kappa\mathcal{S}}\left(1 - \frac{\kappa\mathcal{S}H_0}{m_k}\right) - \beta_{kk}. \tag{24}$$

It can be verified that when the external field is directed along $\mathbf{e}_3$, which is the direction orthogonal to the wire cross-section, both the $\mathbf{H}$ and $\mathbf{B}$ fields are uniform, in particular $\mathbf{H} = H_0\mathbf{e}_3$ (see Appendix A). Therefore, in the wire,

$$\mathbf{M} = \frac{\mathbf{B}}{\mu_0} - H_0\mathbf{e}_3 = \left(\mu_r - 1\right) H_0\mathbf{e}_3, \tag{25}$$

since $\mathbf{B} = \mu_0\mu_r H_0\mathbf{e}_3$, thus

$$m_3 = \left(\mu_r - 1\right)\mathcal{S}H_0. \tag{26}$$

Substituting (26) into (24) yields, after few manipulations,

$$\alpha_{33} = \frac{\mu_0}{\mathcal{S}} - \beta_{33}. \tag{27}$$

V. NUMERICAL VALIDATION OF THE MAGNETOSTATIC FORMULATION

To validate the presented magnetostatic formulation we consider the geometric configurations depicted in Fig. 3. In configuration (a) two parallel infinite wires are separated by a distance Δx_2 along the $\mathbf{e}_2$-direction, whereas in configuration (b) they are separated by Δx_1 along the $\mathbf{e}_1$-direction. An external uniform magnetic field, $\mathbf{H}_0 = 1\mathbf{e}_k$, $k = 1, 2$, is applied, and the magnetic moment per unit length in the wires, $\mathbf{m}$, is computed first from a two-dimensional boundary value problem solved using FEM (the reference solution), and with an implementation of the proposed formulation using the periodic boundary conditions to simulate an infinitely long wire. For symmetry reasons the magnetization, and thus the magnetic moment, are the same in both wires. The relative permeability of the wires is $\mu_r = 300$, and the geometric sizes are $w = 12\text{mm}$ and $d = 3\,mm$.

Fig. 4 and Fig. 5 show the relative error, defined as

$$\text{err} = \frac{\left|\,|m^{(r)}| - |m^{(p)}|\,\right|}{|m^{(r)}|}, \tag{28}$$

where $m^{(r)}$ is the reference value calculated using FEM, whereas $m^{(p)}$ is obtained using the proposed formulation. The horizontal axes in Fig. 4 and Fig. 5 are normalized: in Fig. 4 distance Δx_2 is normalized with respect to the thickness, d, of the wire, whereas in Fig. 5 Δx_1 is normalized with respect to the wire width, w. In test (a) the error is always below 5%, in test (b) it stays permanently below 5% when $\Delta x_1/w \gtrsim 0.16$.

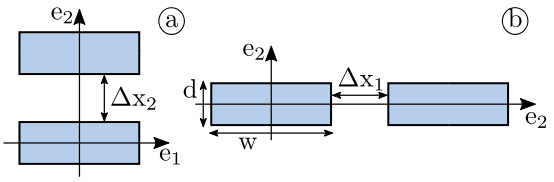

FIGURE 3. Geometric configurations for the validation of the magnetostatic formulation.

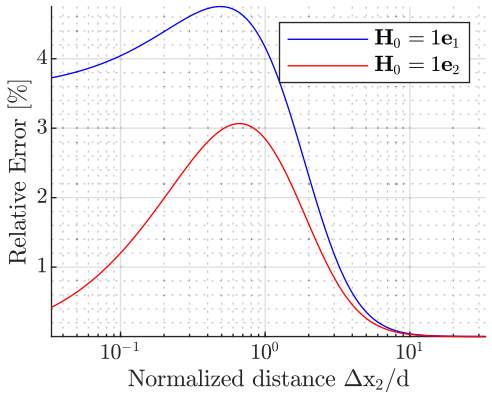

FIGURE 4. Relative error of the magnetostatic test (a).

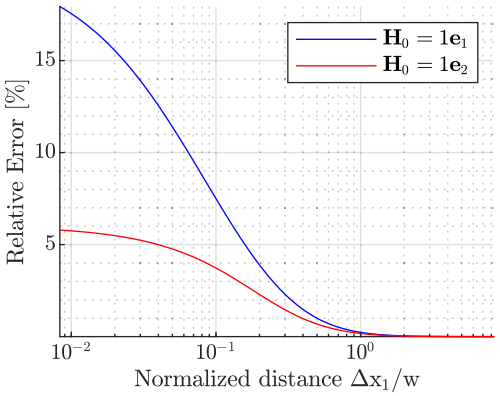

FIGURE 5. Relative error of the magnetostatic test (b).

VI. TIME-HARMONIC FORMULATION FOR A SINGLE WIRE

In time-harmonic conditions it is possible to follow the same approach of [5] and [6], which allows to exploit the magnetostatic formulation presented in section II upon, first of all, defining

$$\mathbf{m}_M = \int_S \mathbf{M}\left(\mathbf{x}'\right) d^2x', \tag{29}$$

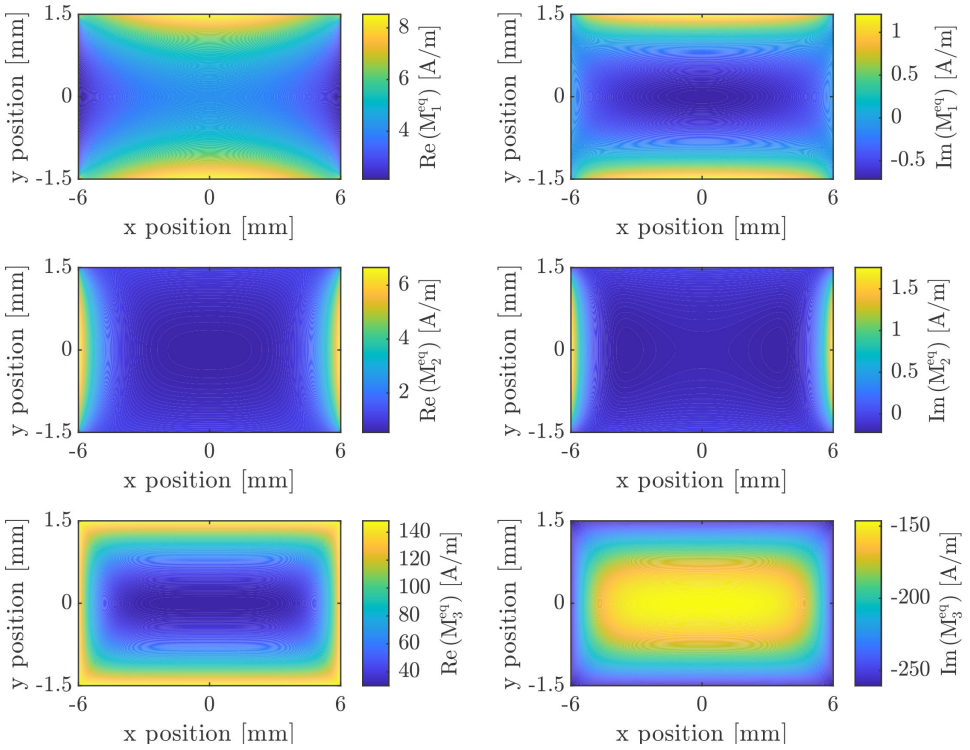

FIGURE 6. Distribution of $\mathbf{M^{eq}(x)} = \mathbf{M(x)} + \frac{1}{2}\,\mathbf{x} \times \mathbf{J(x)}$ over the cross-section of a rectangular wire at 50 Hz, $w = 12\,mm$ and $d = 3\,mm$. The real and imaginary parts of component M_k^{eq} are shown when the external field is directed along $\mathbf{e}_k$.

and

$$\mathbf{m}_J = \frac{1}{2}\int_S \mathbf{x}' \times \mathbf{J}\left(\mathbf{x}'\right) d^2x', \tag{30}$$

where $\mathbf{J}$ is the zero-mean eddy current density induced in the wire cross-section. The total magnetic moment is then intended as

$$\mathbf{m} = \mathbf{m}_M + \mathbf{m}_J. \tag{31}$$

It must be observed that all quantities in these and subsequent equations are complex-valued vector fields, i.e., phasors. The same symbols of the magnetostatic formulation are used for the sake of simplicity.

With definition (31) the same formalism of section III for the discretization can be adopted. Therefore, let us apply a collocation method with constant elements in the wire. In the i-th cuboid the k-th component of the magnetic moment is given by

$$m_k^{(i)} = \frac{\kappa_k \mathcal{S}}{\mu_0} B_k^{(i)}, \tag{32}$$

where $B_k^{(i)}$ is the k-th component of the total field applied in $\mathbf{x}^{(i)}$ and $\kappa_k = 1 - 1/\mu_k$ is a complex coefficient. In case of round wires coefficients κ_k can be calculated analytically [5], [8]. With rectangular wires a numerical approach is required. In particular, by solving a two-dimensional boundary value problem in the case of an infinite straight wire with an external magnetic field imposed along direction $\mathbf{e}_k$, it is possible to define

$$\kappa_k = \frac{\mu_0}{\mathcal{S}} \frac{m_k}{\langle B_k \rangle}, \tag{33}$$

where

$$\langle B_k \rangle = \frac{1}{\mathcal{S}} \int_S B_k\left(\mathbf{x}'\right) d^2x'. \tag{34}$$

The necessity of using (34) stems from the fact that fields $\mathbf{M}$, $\mathbf{J}$ and $\mathbf{B}$ are not uniform over the cross-section, as highlighted for example by Fig. 6. Moreover, FEM simulations show that when the external field is directed along $\mathbf{e}_k$ the components of $\mathbf{m}$ in the orthogonal directions is negligible ($m_{j\neq k} = 0$). Therefore, in the time-harmonic case (6) becomes

$$\mathbf{m}^{(i)} = \frac{\mathcal{S}}{\mu_0} K' \left(\mathbf{B}_0^{(i)} + \mathbf{B}_M^{(i)}\right), \tag{35}$$

with

$$K' = \mathrm{diag}\left(\kappa_1, \kappa_2, \kappa_3\right). \tag{36}$$

Therefore, the linear system of equations (15) becomes

$$\left(I - \frac{\mathcal{S}}{\mu_0} KA\right) \mathbf{u} = \frac{\mathcal{S}}{\mu_0} K \mathbf{b}, \tag{37}$$

where $K \in \mathbb{R}^{3n\times 3n}$ is a block diagonal matrix with matrices K' on its main diagonal:

$$K = \mathrm{diag}\left(K', \ldots, K'\right). \tag{38}$$

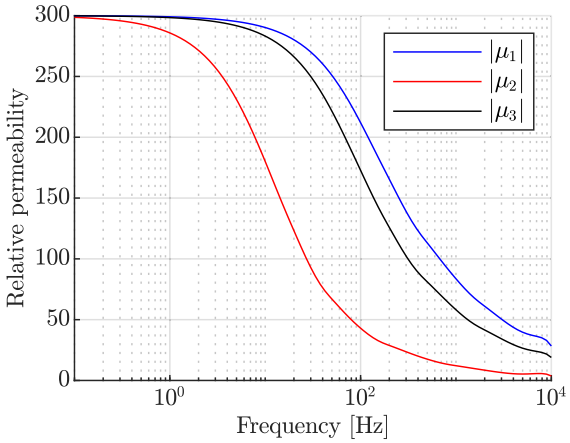

FIGURE 7. Frequency characteristic of $|\mu_1|$, $|\mu_2|$, and $|\mu_3|$. At low frequency all the permeabilities approach the magnetostatic value.

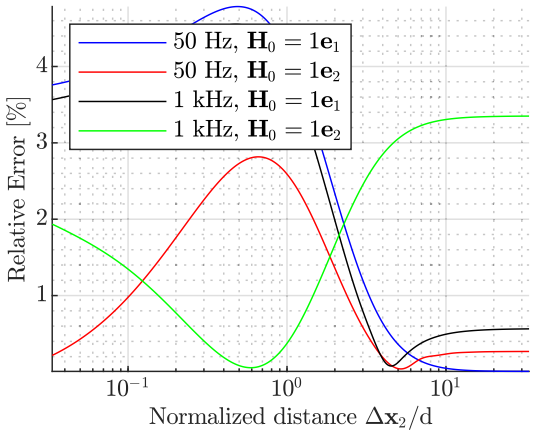

FIGURE 8. Relative error on the magnetic moment magnitude for the time harmonic test with configuration (a) in Fig. 3.

VII. NUMERICAL VALIDATION OF THE TIME-HARMONIC FORMULATION

The validation of the time-harmonic formulation goes through the corresponding tests run for the magnetostatic formulation (section V), described by Fig. 3, in which two parallel infinite rectangular wires are immersed in an external uniform time-harmonic magnetic field. The complex relative permeability is $\mu_r = 300\exp(-j\pi/3)$, the electrical conductivity is $\sigma = 7.246 \cdot 10^6\, S/m$, and the geometric sizes are those of the magnetostatic test. The tests are run at two different frequencies, namely 50 Hz and 1 kHz. Fig. 7 shows the behaviour, in frequency, of the relative permeabilities μ_k. The results of the tests are shown in Fig. 8 and Fig. 9.

A comparison with the tests of the magnetostatic formulation, Fig. 4 and Fig. 5, highlights that in the magnetostatic case the error approaches zero when the distance between wires increases. This occurs because in magnetostatics the fields' distributions in the wires approach those of an isolated wire in a uniform external field, which is the condition in which the coefficients α_{kk} of the self-element were calculated in section IV. In the time-harmonic case coefficients κ_k defined in (33) introduce a modelling error regardless of the distance between the wires, hence the error does not go to zero.

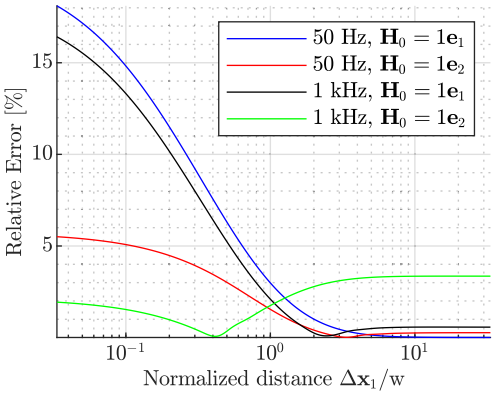

FIGURE 9. Relative error on the magnetic moment magnitude time harmonic test with configuration (b) in Fig. 3.

TABLE 1. Asymptotic errors of the time-harmonic tests. Both tests give, approximately, the same asymptotic errors.

Test	Frequency	$\mathbf{H}_0$	Asymptotic error
(a), (b)	50 Hz	$1\mathbf{e}_1$	∼0.01%
	1 kHz		∼0.6%
	50 Hz	$1\mathbf{e}_2$	∼0.3%
	1 kHz		∼3.4%

Table 1 shows the relative asymptotic errors at 50 Hz and 1 kHz. Such errors are acceptable for the application at hand.

VIII. APPLICATION TO ARMOURED AC SUBMARINE CABLES

As a final step, the proposed method is applied to the case study of an armoured AC submarine cable, Fig. 10, where the mesh of the corresponding cable model is reported. The cable is constituted by three helically-wounded phase conductors, each one carrying the nominal current, that generate a time-harmonic magnetic field: this structure is similar to the one treated in [4], where round armour wires have been replaced with rectangular ones. The magnetic field generated by the phase conductors magnetizes the armour wires and induces eddy currents. The armour wires follow an helicoidal path as well, with a different pitch.

The formulation was tested on two different cable models, whose parameters are summarized in Table 2.

Each model was first solved using FEM with a common software (COMSOL Multiphysics®), which required a 3D mesh such as that shown in Fig. 10 for cable model 1, and a cable 3 times the cross-pitch long, [12]. The solution through the proposed formulation, on the other hand, requires a discretization of the armour only, using cuboids with $d = 3$mm, $w = 12$mm and $h = 12$mm. Fig. 11 shows a portion of the discretized armour for cable model 1. The proposed

TABLE 2. Parameters of the cables.

Parameters	Cable model 1	Cable model 2
Nominal rms current	165 A	790 A
Phase wires helix radius, r_{ph}	37.205 mm	40.87 mm
Phase wires helix pitch	1955.5 mm	2091.9 mm
Armour wires helix radius, r_a	85.73 mm	91.325 mm
Armour wires helix pitch	-3799.3 mm	-2150.0 mm
Number of armour wires, N	21	22
Armour wires width, w	12 mm	
Armour wires thickness, d	3 mm	
Frequency, f	50 Hz	
Armour wires conductivity	$4.673 \cdot 10^6$ S/m	
Armour wires permeability, μ_r	$300 \exp\left(-\mathrm{j}\frac{\pi}{3}\right)$	

TABLE 3. Results of the test on armoured cables.

		Cable model 1	Cable model 2
Losses	FEM	0.397 W/m	12.570 W/m
	Proposed	0.374 W/m	12.021 W/m
	Error	6.16 %	4.57 %
time	FEM	6 h 50 min	4 h 45 min
	Proposed	8 s	8 s

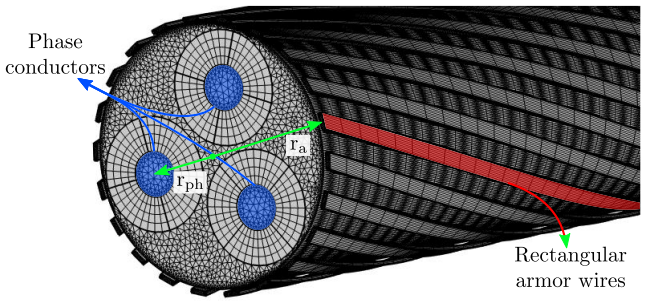

FIGURE 10. FEM mesh of cable model 1.

formulation exploits the helicoidal symmetries described in [12] to reduce the computational burden.

In the armour the rectangular wires are spread along a circle. In order to use the validation results of section VII, $\Delta x_1/w$ (Fig. 3) can be estimated, with the help of Fig. 12, as:

$$\frac{\Delta x_1}{w} \simeq \frac{r_a\theta - w}{w} = \frac{2\pi r_a}{Nw} - 1, \tag{39}$$

where r_a is the radius of the armour and N is the number of armour wires. For cable model 1 such a ratio is 1.4, whereas for cable model 2 it is 1.2. These values are greater than 1 and they corresponds to small errors, as it can be seen from Fig. 9.

Table 3 compares the total armour losses obtained from FEM with those obtained from the proposed integral formulation. The total losses are calculated by summing the electric (Joule) and magnetic (hysteresis) losses in each wire. In particular, the electric and magnetic losses per unit length

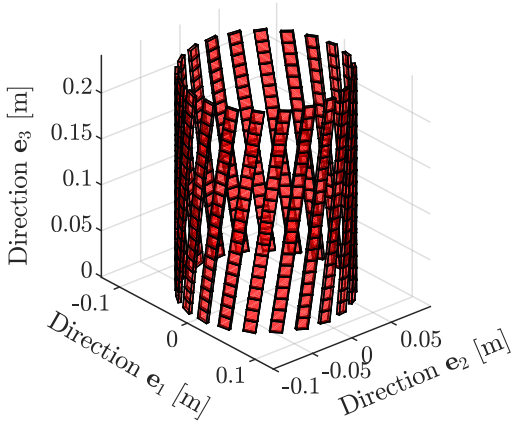

FIGURE 11. Armour discretization with 12 mm × 3 mm × 12 mm cuboids for model cable 1.

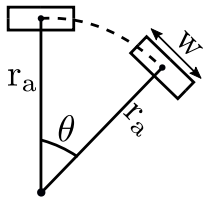

FIGURE 12. Sketch of the armour geometry.

are calculated as, [4],

$$P_r = \sigma \int_S |\mathbf{E}|^2 \, \mathrm{d}S, \tag{40}$$

$$P_m = Re\left\{j\omega\mu_0\mu_r\right\} \int_S |\mathbf{H}|^2 \, \mathrm{d}S, \tag{41}$$

where recall that S is the wire cross-section. The total wire loss is $P_w = P_e + P_m$. It was shown in [4] that, due to the linearity, both $\mathbf{E}$ and $\mathbf{H}$ are proportional the externally applied uniform field $\mathbf{B}_0$. Thus, also the magnetic moment, $\mathbf{m}$, is proportional to $\mathbf{B}_0$. Then, the total loss of each rectangular wire can be calculated as,

$$P_w = h \sum_{j=1}^{n} \sum_{k=1}^{3} \left(c_{k,e} + c_{k,m}\right) \left|m_k^{(j)}\right|^2, \tag{42}$$

where n is the number of cuboids in which the wire is discretized, h is the height of each cuboid, $m_k^{(j)}$ is the k-th component of the magnetic moment in the j-th cuboid, $c_{j,e}$ and $c_{j,m}$ are the loss coefficients for the electric and magnetic losses, respectively. Such coefficients can be calculated analytically in the case of a round wire, [4], whereas for a rectangular wire they are obtained by solving with FEM a 2D boundary value problem in which the wire is assumed to be infinitely long. Specifically, coefficients in (42) are calculated as follows: an external magnetic flux density is applied along $\mathbf{e}_k$, $\mathbf{B}_0 = \mu_0\mathbf{e}_k$, then the total electric and magnetic losses on the cross-section, $p_{e,k}$ and $p_{m,k}$ respectively, are computed,

and finally $c_{k,e}$ and $c_{k,m}$ are obtained as

$$c_{k,e} = \frac{p_{e,k}}{|m_k|^2} \quad \text{and} \quad c_{k,m} = \frac{p_{m,k}}{|m_k|^2}, \tag{43}$$

where m_k is the k-th component of the magnetic moment.

From Table 3 it can be observed that the errors are below 7 % which, considering the approximations behind the proposed formulation, can be considered as an acceptable result. Moreover, the computational time required by the proposed formulation, in which the calculation is efficiently handled exploiting the helicoidal symmetries described in [12], is about 8 s, whereas the FEM calculation requires between 4 h 45 min and 6 h 50 min, depending on the cable model.

IX. CONCLUSION

This paper proposes an integral formulation for the calculation of power losses in rectangular wires. First, the formulation is treated in the magnetostatic limit. A method for calculating the self-element by avoiding the solution of a 3D boundary value problem is proposed. Then the formulation is extended to the time-harmonic case. The numerical tests in both the magnetostatic and time-harmonic conditions show that the accuracy increases as the distance between the wires increases. A final test on armoured AC submarine power cables shows that the proposed method is sufficiently accurate in the calculation of the armour losses, and it significantly reduces the computational time with respect to FEM.

The presented formulation has been tested on two geometric structures: infinitely straight wires and helically-wrapped wires. Another interesting case would be that of planar structures, such as those found in planar transformers [13]. In this case, however, the formulation should be modified in order to take into account the non-zero mean currents that flow in the windings. The presented formulation for rectangular wires could be then extended as done in [6] for round wires.

APPENDIX A
PROPERTIES OF A_S AND A_E

The self-element calculation detailed in section IV relies on the fact that the infinite series defining A_e is convergent, and that both A_e and A_s are diagonal matrices.

A. PROOF OF THE CONVERGENCE

Matrix A_e is given by the infinite series in (21). To prove its convergence, recalling (14) and letting $\mathbf{v}(\mathbf{x}') = (\mathbf{x}^{(0)} - \mathbf{x}')/|\mathbf{x}^{(0)} - \mathbf{x}'|$, the integral in (11) can be rewritten, for $i = 0$ and $k = 1, 2, 3$, as

$$\mathbf{a}_k^{(0,j)} = -\frac{\mu_0}{4\pi} \int_{\partial\Omega_M^{(j)}} \left(\mathbf{n}(\mathbf{x}') \times \frac{\mathbf{e}_k}{\mathcal{S}}\right) \times \frac{\mathbf{v}(\mathbf{x}')}{|\mathbf{x}^{(0)} - \mathbf{x}'|^2} d^2x'. \tag{44}$$

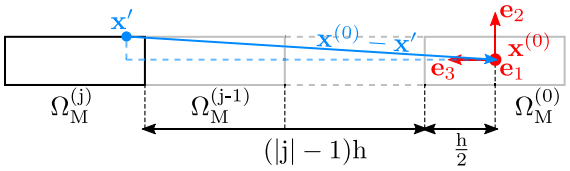

FIGURE 13. Side view of the infinite straight wire to explain the inequality in (45).

Given that (see Fig. 13)

$$|\mathbf{x}^{(0)} - \mathbf{x}'| \geq \left(|j| - \frac{1}{2}\right) h \qquad \text{for } j \neq 0, \tag{45}$$

the series' terms can be bounded as

$$\begin{aligned} \left|\mathbf{a}_k^{(0,j)}\right| &\leq \frac{\mu_0/(4\pi)}{\left(|j| - \frac{1}{2}\right)^2 h^2} \int_{\partial\Omega_M^{(j)}} \left|\left(\mathbf{n}(\mathbf{x}') \times \frac{\mathbf{e}_k}{\mathcal{S}}\right) \times \mathbf{v}(\mathbf{x}')\right| d^2x' \\ &\leq \frac{c}{\left(|j| - \frac{1}{2}\right)^2}, \end{aligned} \tag{46}$$

because the integral is finite. From (46) it follows that, for $k = 1, 2, 3$,

$$\left|\sum_{j\in\mathbb{Z}\setminus\{0\}} \mathbf{a}_k^{(0,j)}\right| \leq \sum_{j\in\mathbb{Z}\setminus\{0\}} \left|\mathbf{a}_k^{(0,j)}\right| \leq \sum_{j\in\mathbb{Z}\setminus\{0\}} \frac{c}{\left(|j| - \frac{1}{2}\right)^2}. \tag{47}$$

Since $c/(|j| - 1/2)^2 \sim c/j^2$ the last series converges, hence A_e is finite.

B. PROOF THAT A_E IS DIAGONAL

The columns of matrices $A^{(0,j)}$ that contribute to A_e through the infinite series (21) are given by (44). Matrix A_e is diagonal if and only if, for $k = 1, 2, 3$, its k-th columns is a vector parallel to $\mathbf{e}_k$. To state this fact properly, let

$$A_e = [\mathbf{a}_1 \quad \mathbf{a}_2 \quad \mathbf{a}_3], \tag{48}$$

with the k-th column vector given by

$$\mathbf{a}_k = \sum_{j\in\mathbb{Z}\setminus\{0\}} \mathbf{a}_k^{(0,j)}. \tag{49}$$

Evidently, in order for A_e to be diagonal the following relationship must hold:

$$\mathbf{a}_k \parallel \mathbf{e}_k \text{ (i.e., } \mathbf{a}_k \times \mathbf{e}_k = 0) \quad \forall k = 1, 2, 3. \tag{50}$$

The objective then is to prove this last statement.

Before tackling the general proof it is worth going through some observations. The argument relies on the properties of the integrand function

$$\boldsymbol{\psi}_k(\mathbf{x}') = \left(\mathbf{n}(\mathbf{x}') \times \mathbf{e}_k\right) \times \frac{\mathbf{v}(\mathbf{x}')}{|\mathbf{x}^{(0)} - \mathbf{x}'|^2}, \tag{51}$$

where the cross-section area, $\mathcal{S}$, has been omitted since it does not affect the behaviour of $\boldsymbol{\psi}_k(\mathbf{x}')$. From Fig. 14 it is immediate to see that the normal versor, $\mathbf{n}(\mathbf{x}')$, is always

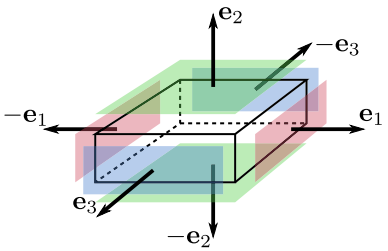

FIGURE 14. Faces of the rectangular cuboid with their corresponding normal versors.

parallel to one of the $\mathbf{e}_k$. In particular, the product $\mathbf{n}(\mathbf{x}') \times \mathbf{e}_k$ can take the following non-null forms:

$$\pm\mathbf{e}_3 \times \mathbf{e}_1 = \pm\mathbf{e}_2, \tag{52}$$
$$\pm\mathbf{e}_2 \times \mathbf{e}_1 = \mp\mathbf{e}_3, \tag{53}$$
$$\pm\mathbf{e}_1 \times \mathbf{e}_2 = \pm\mathbf{e}_3, \tag{54}$$
$$\pm\mathbf{e}_3 \times \mathbf{e}_2 = \mp\mathbf{e}_1, \tag{55}$$
$$\pm\mathbf{e}_2 \times \mathbf{e}_3 = \pm\mathbf{e}_1, \tag{56}$$
$$\pm\mathbf{e}_1 \times \mathbf{e}_3 = \mp\mathbf{e}_2. \tag{57}$$

The above relationships can be written in a more compact way. Let $m, k, p \in \{1, 2, 3\}$ such that $m \neq k \neq p$, and let $\mathbf{n}(\mathbf{x}') = \mathbf{e}_m$, then

$$\mathbf{e}_m \times \mathbf{e}_k = (-1)^{\lambda_{mk}} \mathbf{e}_p, \tag{58}$$

where we defined the following map:

$$\lambda_{mk} = \begin{cases} 0 & \text{if } (m+1) \bmod 3 = k, \\ 1 & \text{if } (k+1) \bmod 3 = m. \end{cases} \tag{59}$$

Map λ_{mk} has some simple properties that will be useful later. For $\alpha, \beta, \gamma \in \{1, 2, 3\}$ such that $\alpha \neq \beta \neq \gamma$,

$$\lambda_{\alpha\beta} + \lambda_{\beta\alpha} = 1, \tag{60}$$
$$\lambda_{\alpha\beta} + \lambda_{\alpha\gamma} = 1. \tag{61}$$

Looking back at (51), the result of the first cross product is then multiplied by $\mathbf{v}(\mathbf{x}')$. Let, for example, be $m = 1$ and $k = 3$, and let $\mathbf{v}(\mathbf{x}') = v_1\mathbf{e}_1 + v_2\mathbf{e}_2 + v_3\mathbf{e}_3$. It follows from (58) that

$$(\mathbf{e}_1 \times \mathbf{e}_3) \times \mathbf{v}(\mathbf{x}') = -\mathbf{e}_2 \times \mathbf{v}(\mathbf{x}') = -v_3\mathbf{e}_1 + v_1\mathbf{e}_3, \tag{62}$$
$$(-\mathbf{e}_1 \times \mathbf{e}_3) \times \mathbf{v}(\mathbf{x}') = \mathbf{e}_2 \times \mathbf{v}(\mathbf{x}') = \quad v_3\mathbf{e}_1 - v_1\mathbf{e}_3. \tag{63}$$

Referring to Fig. 15, $-\mathbf{e}_2 \times \mathbf{v}(\mathbf{x}')$ corresponds to a projection of $\mathbf{v}(\mathbf{x}')$ on a plane perpendicular to $\mathbf{e}_2$, followed by a rotation of $+\pi/2$ around $\mathbf{e}_2$ itself. In Fig. 15 vector $\mathbf{v}_a$ is rotated by $+pi/2$. On the contrary, $-\mathbf{e}_2 \times \mathbf{v}(\mathbf{x}')$ corresponds to a rotation of $-\pi/2$ around $\mathbf{e}_2$. In Fig. 15 vector $\mathbf{v}_b$ is the reflection of $\mathbf{v}_a$ with respect to axis s (thus $|\mathbf{v}_b| = |\mathbf{v}_a|$), and it is rotated by $-\pi/2$ around $\mathbf{e}_2$. It is important to note that the sum $-\mathbf{e}_2 \times \mathbf{v}_a + \mathbf{e}_2 \times \mathbf{v}_b$ results in a vector parallel to $\mathbf{e}_3$, which is the versor corresponding to the initial choice of k in this example.

The above example suggests the presence of geometric symmetries in the infinite straight wire. Fig. 16 shows the three symmetry planes Π_1, Π_2, and Π_3, such that $\Pi_m \perp \mathbf{e}_m$,

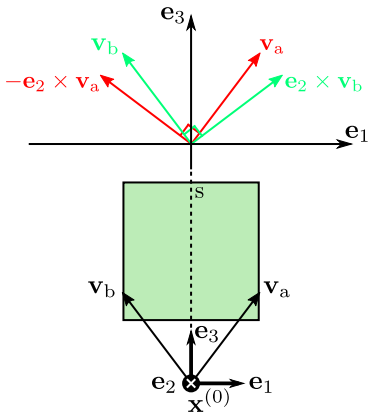

FIGURE 15. Examples of rotations described by equations (63) and (63).

that intersect each other in $\mathbf{x}^{(0)}$. In the following, being $\mathbf{w} \in \mathbb{R}^3$ a vector with its origin in $\mathbf{x}^{(0)}$, we will indicate with $\rho_k(\mathbf{w})$ the reflection of $\mathbf{w}$ with respect Π_k.

At this point we are ready to present a formal proof of (50). Let $m, k, p \in \{1, 2, 3\}$ such that $m \neq k \neq p$, and let $\mathbf{t}, \mathbf{u}, \mathbf{s} \in \mathbb{R}^3$. We define, being $\mathbf{w} \in \mathbb{R}^3$,

$$\phi_{\mathbf{w}}(\mathbf{t}, \mathbf{u}, \mathbf{s}) = (\mathbf{w} \cdot \mathbf{e}_m)\mathbf{t} + (\mathbf{w} \cdot \mathbf{e}_k)\mathbf{u} + (\mathbf{w} \cdot \mathbf{e}_p)\mathbf{s}. \tag{64}$$

In particular,

$$\mathbf{w} = \phi_{\mathbf{w}}(\mathbf{e}_m, \mathbf{e}_k, \mathbf{e}_p), \tag{65}$$

and its reflection with respect to Π_m is

$$\rho_m(\mathbf{w}) = \phi_{\mathbf{w}}(-\mathbf{e}_m, \mathbf{e}_k, \mathbf{e}_p). \tag{66}$$

Choosing now $\mathbf{x}^{(0)}$ as the origin of the reference frame, letting $\mathbf{n}(\mathbf{x}') = \mathbf{e}_m$ and using (58) and (65), we have

$$\begin{aligned} \boldsymbol{\psi}_k(\mathbf{x}') &= (\mathbf{e}_m \times \mathbf{e}_k) \times \frac{\mathbf{v}(\mathbf{x}')}{|\mathbf{x}'|^2} \\ &= (-1)^{\lambda_{mk}}\, \mathbf{e}_p \times \frac{\phi_{\mathbf{v}(\mathbf{x}')}(\mathbf{e}_m, \mathbf{e}_k, \mathbf{e}_p)}{|\mathbf{x}'|^2} \\ &= (-1)^{\lambda_{mk}}\, \frac{\phi_{\mathbf{v}(\mathbf{x}')}\left(\mathbf{e}_p \times \mathbf{e}_m,\ \mathbf{e}_p \times \mathbf{e}_k,\ \mathbf{e}_p \times \mathbf{e}_p\right)}{|\mathbf{x}'|^2} \\ &= (-1)^{\lambda_{mk}}\, \frac{\phi_{\mathbf{v}(\mathbf{x}')}\left((-1)^{\lambda_{pm}}\, \mathbf{e}_k,\ (-1)^{\lambda_{pk}}\, \mathbf{e}_m,\ \mathbf{0}\right)}{|\mathbf{x}'|^2} \end{aligned} \tag{67}$$

Note that the case $\mathbf{n}(\mathbf{x}') = -\mathbf{e}_m$ must also be taken into consideration, and it leads to a simple reversal of the resulting vector, i.e. $-\boldsymbol{\psi}_k(\mathbf{x}')$. From property (61) it follows that if $\lambda_{pm} = 1$ then $\lambda_{pk} = 0$, or vice versa, hence

$$\begin{aligned} &\phi_{\mathbf{v}(\mathbf{x}')}\left((-1)^{\lambda_{pm}}\, \mathbf{e}_k,\ (-1)^{\lambda_{pk}}\, \mathbf{e}_m,\ \mathbf{0}\right) \\ &= \begin{cases} \phi_{\mathbf{v}(\mathbf{x}')}(-\mathbf{e}_k,\ \ \mathbf{e}_m,\ \mathbf{0}) & \text{if } \lambda_{pm} = 1, \lambda_{pk} = 0, \\ \phi_{\mathbf{v}(\mathbf{x}')}(\ \ \mathbf{e}_k, -\mathbf{e}_m,\ \mathbf{0}) & \text{if } \lambda_{pm} = 0, \lambda_{pk} = 1. \end{cases} \end{aligned} \tag{68}$$

In either case, the result of (68) is a rotation of $\pm\pi/2$ around $\mathbf{e}_p$, as shown by Fig. 17. Term $(-1)^{\lambda_{mk}}$ in (68) has the role of reversing the rotations when $\lambda_{mk} = 1$, but it does not affect the nature of the transformation.

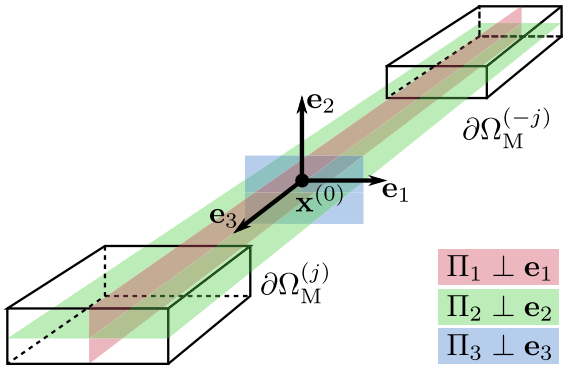

FIGURE 16. Symmetry planes for the infinite straight wire configuration.

Using the definition of $\boldsymbol{\psi}_k(\mathbf{x}')$, (51), the k-th column of A_e, defined in (49), can be written as

$$\mathbf{a}_k = -\frac{\mu_0}{4\pi\mathcal{S}} \sum_{j\in\mathbb{Z}\setminus\{0\}} \int_{\partial\Omega_M^{(j)}} \boldsymbol{\psi}_k(\mathbf{x}')d^2x' \tag{69}$$

Boundary $\partial\Omega_M^{(j)}$ on which the integration is performed can be split into the six faces of the cuboid depicted in Fig. 18:

$$\partial\Omega_M^{(j)} = \bigcup_{m=1}^{3} \Sigma_m^{(j)} \cup \Sigma_{-m}^{(j)}, \tag{70}$$

where the normal to $\Sigma_{\pm m}^{(j)}$ is $\pm\mathbf{e}_m$. In this way (69) can be rewritten as

$$\begin{aligned}\mathbf{a}_k = &-\frac{\mu_0}{4\pi\mathcal{S}} \sum_{j\in\mathbb{Z}\setminus\{0\}} \sum_{m=1}^{3} \int_{\Sigma_m^{(j)}} \boldsymbol{\psi}_k(\mathbf{x}')d^2x' \\ &- \int_{\Sigma_{-m}^{(j)}} \boldsymbol{\psi}_k(\mathbf{y}')d^2y',\end{aligned} \tag{71}$$

where we used the fact that on $\Sigma_{-m}^{(j)}$ the normal is $-\mathbf{e}_m$ and thus the integrand is given by $-\boldsymbol{\psi}_k(\mathbf{y}')$. The integrals in the last expression can be rewritten in a simpler way by exploiting the symmetry planes in Fig. 16. The idea is to exploit suitable reflections that can be visualized with the help of Fig. 19. Two situations can be distinguished:

$$m = 1, 2,\ \mathbf{t} \in \Sigma_{-m}^{(j)} \implies \exists \mathbf{u} \in \Sigma_m^{(j)} \mid \mathbf{t} = \rho_m(\mathbf{u}), \tag{72}$$

$$m = 3,\ \mathbf{t} \in \Sigma_{\pm 3}^{(j)} \implies \exists \mathbf{u} \in \Sigma_{\mp 3}^{(-j)} \mid \mathbf{t} = \rho_3(\mathbf{u}). \tag{73}$$

From (72) it follows that, $\forall j \in \mathbb{Z} \setminus \{0\}$,

$$\begin{aligned}&\sum_{m=1}^{2} \int_{\Sigma_m^{(j)}} \boldsymbol{\psi}_k(\mathbf{x}')d^2x' - \int_{\Sigma_{-m}^{(j)}} \boldsymbol{\psi}_k(\mathbf{y}')d^2y' \\ &\quad = \sum_{m=1}^{2} \int_{\Sigma_m^{(j)}} \Big[\, \boldsymbol{\psi}_k(\mathbf{x}') - \boldsymbol{\psi}_k(\rho_m(\mathbf{x}')) \,\Big] d^2x'.\end{aligned} \tag{74}$$

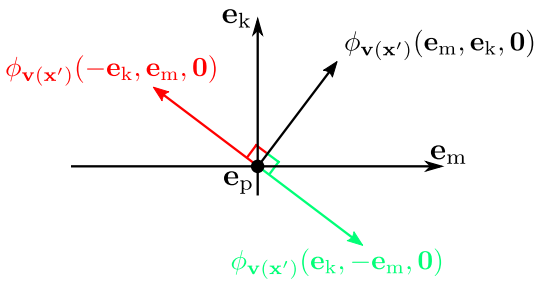

FIGURE 17. Rotations around $\mathbf{e}_k$ on the plane identified by $\mathbf{e}_m$ and $\mathbf{e}_k$. Vector $\phi_{\mathbf{v}}(\mathbf{e}_m, \mathbf{e}_k, \mathbf{0})$ is the projection of $\mathbf{v}(\mathbf{x}')$ on the plane.

The case of (73) requires to consider the terms related to j and $-j$ in order to exploit the symmetry. In particular, $\forall j \in \mathbb{Z}\setminus\{0\}$,

$$\begin{aligned}&\int_{\Sigma_3^{(j)}} \boldsymbol{\psi}_k(\mathbf{x}')d^2x' - \int_{\Sigma_{-3}^{(j)}} \boldsymbol{\psi}_k(\mathbf{x}')d^2x' \\ &\quad + \int_{\Sigma_3^{(-j)}} \boldsymbol{\psi}_k(\mathbf{x}')d^2x' - \int_{\Sigma_{-3}^{(-j)}} \boldsymbol{\psi}_k(\mathbf{x}')d^2x' \\ &\quad = \int_{\Sigma_3^{(j)}} \Big[\, \boldsymbol{\psi}_k(\mathbf{x}') - \boldsymbol{\psi}_k(\rho_3(\mathbf{x}')) \,\Big] d^2x' \\ &\quad - \int_{\Sigma_3^{(-j)}} \Big[\, \boldsymbol{\psi}_k(\mathbf{x}') - \boldsymbol{\psi}_k(\rho_3(\mathbf{x}')) \,\Big] d^2x'.\end{aligned} \tag{75}$$

It is important to observe that the operations in (75) require a permutation of the series terms. The fact that the final result of the series does not change after such a permutation is guaranteed by the absolute convergence.

Using (74) and (75) it is possible to rewrite (71) as

$$\mathbf{a}_k = -\frac{\mu_0}{4\pi\mathcal{S}} \sum_{j\in\mathbb{Z}\setminus\{0\}} \sum_{m=1}^{3} \int_{\Sigma_m^{(-j)}} \Big[\boldsymbol{\psi}_k(\mathbf{x}') - \boldsymbol{\psi}_k(\rho_m(\mathbf{x}'))\Big] d^2x'. \tag{76}$$

Using (66) and going through the same steps as in (67), it is possible to show that

$$\boldsymbol{\psi}_k(\mathbf{x}') = (-1)^{\lambda_{mk}} \frac{\phi_{\mathbf{v}(\mathbf{x}')}\Big(-(-1)^{\lambda_{pm}}\mathbf{e}_k,\ (-1)^{\lambda_{pk}}\mathbf{e}_m,\ \mathbf{0}\Big)}{|\mathbf{x}'|^2} \tag{77}$$

and this means that

$$\boldsymbol{\psi}_k(\mathbf{x}') - \boldsymbol{\psi}_k(\rho_m(\mathbf{x}')) = (-1)^{\lambda_{mk}} \frac{\phi_{\mathbf{v}(\mathbf{x}')}\Big((-1)^{\lambda_{pm}}2\mathbf{e}_k,\ \mathbf{0},\ \mathbf{0}\Big)}{|\mathbf{x}'|^2}. \tag{78}$$

In conclusion,

$$\boldsymbol{\psi}_k(\mathbf{x}') - \boldsymbol{\psi}_k(\rho_m(\mathbf{x}')) \parallel \mathbf{e}_k \implies \mathbf{a}_k \parallel \mathbf{e}_k \quad \forall\, k = 1, 2, 3, \tag{79}$$

hence (50) is demonstrated.

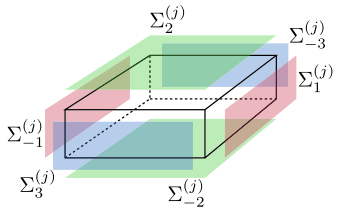

FIGURE 18. Faces of the cuboid on which the integration is performed.

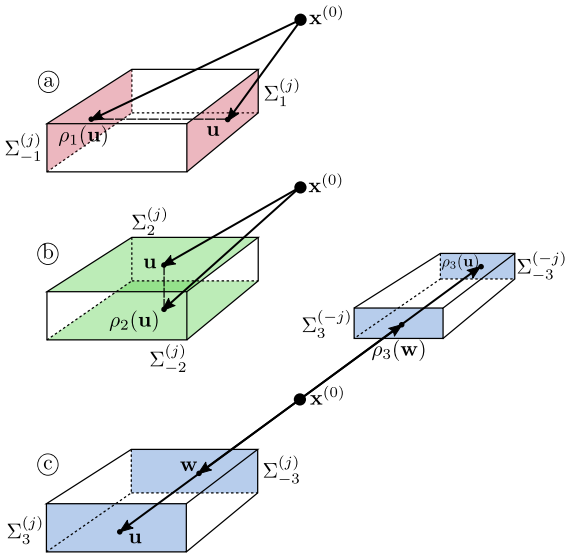

FIGURE 19. Reflections with respect to the symmetry planes (not indicated here for clarity, refer to Fig. 16). (a) Reflection with respect to Π_1. (b) Reflection with respect to Π_2. (c) Reflection with respect to Π_3.

C. PROOF THAT A_S IS DIAGONAL

Matrix A_s is calculated indirectly from (22), that is rewritten here for the sake of convenience as

$$\left(\mathrm{I} - \frac{\kappa\mathcal{S}}{\mu_0}(A_s + A_e)\right)\mathbf{m} = \frac{\kappa\mathcal{S}}{\mu_0}\mathbf{B}_0. \tag{80}$$

The procedure in section IV assumed that when the external field $\mathbf{B}_0$ was uniform and parallel to $\mathbf{e}_k$, e.g., $\mathbf{B}_0 = \mu_0 H_0 \mathbf{e}_k$, then the magnetic moment per unit length, $\mathbf{m}$, in the infinite straight wire was parallel to $\mathbf{e}_k$ as well. In this way, since A_e is diagonal it follows that A_s must be diagonal.

The two-dimensional magnetostatic problem can be stated, in the wire domain Ω_M, as

$$\nabla \times \mathbf{H} = \mathbf{0}, \tag{81}$$
$$\nabla \cdot \left(\mu_0 \mu_r \mathbf{H}\right) = 0. \tag{82}$$

Since $\mathbf{H}$ is irrotational it admits a scalar potential ψ such that $\mathbf{H} = -\nabla\psi$. In particular, ψ satisfies the Laplace equation, $\nabla^2\psi = 0$. Being $\mathbf{M} = (\mu_r - 1)\mathbf{H}$ the magnetization in the wire, the magnetic moment per unit length can be written as

$$\mathbf{m} = \int_S \mathbf{M}\, d\,S = -(\mu_r - 1)\int_S \nabla\psi\, d\,S, \tag{83}$$

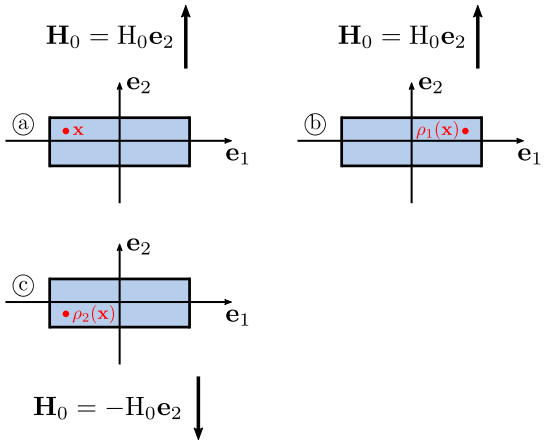

FIGURE 20. Symmetries when the external field is parallel to $\mathbf{e}_2$. (a) Reference case. (b) Rotation around axis $\mathbf{e}_2$. (c) Rotation around axis $\mathbf{e}_1$. (d) Rotation around axis $\mathbf{e}_3$.

where in particular for the j-th component of $\mathbf{m}$ it holds

$$m_j = -(\mu_r - 1)\int_S \frac{\partial\psi}{\partial x_j}\, d\,S. \tag{84}$$

Therefore, the statement to be proven is that if the external magnetic field is $\mathbf{H}_0 = H_0\mathbf{e}_k$ then all the components of $\mathbf{m}$ except for the k-th must vanish. In turn, based on (84), this must follow from the properties of ψ.

Let us first consider cases $k = 1$ and $k = 2$, that are formally the same. Let us refer to the latter then: it will be sufficient to understand the general implications. Case (a) in Fig. 20 depicts the cross-section of the rectangular wire immersed in a uniform external field $\mathbf{H}_0 = H_0\mathbf{e}_2$. In particular, point $\mathbf{x}$ lies in the third quadrant of the plane. If the geometry is rotated around axis $\mathbf{e}_2$ by 180°, as shown in case (b) of Fig. 20, point $\mathbf{x}$ ends up in $\rho_1(\mathbf{x})$. Cases (a) and (b) are equivalent, in the sense that they have the same geometry, with the same external field. Being $\mathbf{x} = x_1\mathbf{e}_1 + x_2\mathbf{e}_2$, this means that

$$\psi(\mathbf{x}) = \psi(x_1, x_2) = \psi(-x_1, x_2) = \psi(\rho_1(\mathbf{x})), \tag{85}$$

or in other words that ψ is even with respect to coordinate x_1. Case (c) in Fig. 20 shows a rotation around axis $\mathbf{e}_1$, hence point $\mathbf{x}$ of case (a) ends up onto point $\rho_2(\mathbf{x})$. This situation is different, because even though the geometry is still the same, the external field is reversed with respect to case (a): $\mathbf{H}_0 = -H_0\mathbf{e}_2$. This means that ψ is odd with respect to coordinate x_2:

$$\psi(\mathbf{x}) = \psi(x_1, x_2) = -\psi(x_1, -x_2) = -\psi(\rho_2(\mathbf{x})). \tag{86}$$

Using now (84), the even symmetry (85) implies that

$$\begin{aligned} m_1 &= -(\mu_r - 1)\int_{-\frac{d}{2}}^{\frac{d}{2}} dx_2 \int_{-\frac{w}{2}}^{\frac{w}{2}} dx_1\, \frac{\partial\psi}{\partial x_1} \\ &= -(\mu_r - 1)\int_{-\frac{d}{2}}^{\frac{d}{2}} dx_2 \left[\psi\left(\frac{w}{2}, x_2\right) - \psi\left(-\frac{w}{2}, x_2\right)\right] \\ &= 0. \end{aligned} \tag{87}$$

On the other hand, the odd symmetry (86) implies

$$m_2 = \int_{-\frac{w}{2}}^{\frac{w}{2}} dx_1\, 2\,\psi\left(x_1, \frac{d}{2}\right), \tag{88}$$

which is in general different from zero.The same argument can be adapted to the case of a field parallel to $\mathbf{e}_1$, and brings to the conclusion that $m_2 = 0$ and $m_1 \neq 0$.

For the case $k = 3$, several numerical tests have shown that the field is always parallel to the external one. In this situation it can be verified that $\psi(\mathbf{x}) = -H_0 x_3$ is a solution of the Laplace equation with the external field $\mathbf{H}_0 = H_0\mathbf{e}_3$, which implies that the magnetic field in the wire is uniform: $\mathbf{H} = -\nabla\psi = H_0\mathbf{e}_3$. This means that the magnetic moment in the wire is

$$\mathbf{m} = \mathbf{M}\mathcal{S} = (\mu_r - 1)\mathbf{H}\mathcal{S} = (\mu_r - 1)\mathcal{S}H_0\mathbf{e}_3. \tag{89}$$

In conclusion, for a field parallel to $\mathbf{e}_k$, the resulting magnetic moment $\mathbf{m}$ is parallel to $\mathbf{e}_k$ as well. From (80), given that A_e is diagonal, it follows that A_s is diagonal.

REFERENCES

[1] K. Zhang, Y. Liang, X. Bian, and P. Yang, "Torque analytical calculation of formed winding permanent magnet motor," *IEEE Access*, vol. 11, pp. 36702–36712, 2023.

[2] J. Smajic, J. Hughes, T. Steinmetz, D. Pusch, W. Monig, and M. Carlen, "Numerical computation of ohmic and eddy-current winding losses of converter transformers including higher harmonics of load current," *IEEE Trans. Magn.*, vol. 48, no. 2, pp. 827–830, Feb. 2012.

[3] X. Ou, W. XU, Y. Zang, H. Wang, H. Wu, A. Lv, and Z. Zhou, "Mechanical analysis of 500 kV oil-filled submarine power cable in anchor and blade damage based on finite element method," in *Proc. IEEE 6th Adv. Inf. Technol., Electron. Autom. Control Conf. (IAEAC)*, Oct. 2022, pp. 1068–1072.

[4] L. Giussani, L. Di Rienzo, M. Bechis, and C. de Falco, "Computation of armor losses in AC submarine cables," *IEEE Trans. Power Del.*, vol. 36, no. 5, pp. 3014–3021, Oct. 2021.

[5] L. Giussani, M. Bechis, C. de Falco, and L. Di Rienzo, "An integral formulation for an array of wires in a 3-D magneto-quasi-static field," *IEEE Trans. Magn.*, vol. 54, no. 7, pp. 1–8, Jul. 2018.

[6] L. Giussani, L. Di Rienzo, and C. de Falco, "Integral formulation for magnetic and conductive wire loops in an external time-harmonic magnetoquasi-static field," *IEEE Trans. Magn.*, vol. 55, no. 11, pp. 1–4, Nov. 2019.

[7] L. Giussani, L. Di Rienzo, M. Bechis, and C. de Falco, "Fully coupled computation of losses in metallic sheaths and armor of AC submarine cables," *IEEE Trans. Power Del.*, vol. 37, no. 5, pp. 3803–3812, Oct. 2022.

[8] H. Igarashi, "Semi-analytical approach for finite-element analysis of multi-turn coil considering skin and proximity effects," *IEEE Trans. Magn.*, vol. 53, no. 1, pp. 1–7, Jan. 2017.

[9] S. Hiruma and H. Igarashi, "Fast 3-D analysis of eddy current in Litz wire using integral equation," *IEEE Trans. Magn.*, vol. 53, no. 6, pp. 1–4, Jun. 2017.

[10] J. D. Jackson, *Classical Electrodynamics*, 2nd ed. Hoboken, NJ, USA: Wiley, 1975, ch. 5.

[11] J. A. Stratton, *Electromagnetic Theory*. New York, NY, USA: McGraw-Hill, 1941, pp. 258–261.

[12] L. Giussani, L. Di Rienzo, M. Bechis, and C. de Falco, "Losses computation in thin conductive sheaths of power cables via an integral approach," *IEEE Trans. Magn.*, vol. 57, no. 6, pp. 1–4, Jun. 2021.

[13] C.-W. Park and S.-K. Han, "Analysis and design of an integrated magnetics planar transformer for high power density LLC resonant converter," *IEEE Access*, vol. 9, pp. 157499–157511, 2021.

PASQUALE CAMBARERI was born in Busto Arsizio, Italy, in 1992. He received the M.Sc. and Ph.D. degrees in electrical engineering from Politecnico di Milano, in 2019 and 2023, respectively. His research interests include numerical methods for electromagnetic fields, and modeling of electrical insulating materials.

LUCA DI RIENZO (Senior Member, IEEE) received the Laurea (M.Sc.) (cum laude) and Ph.D. degrees in electrical engineering from Politecnico di Milano, in 1996 and 2001, respectively, and the B.S. degree (cum laude) in mathematics from università Statale di Milano, in 2020. He is currently an Associate Professor with Dipartimento di Elettronica, Informazione e Bioingegneria, Politecnico di Milano. His research interests are in computational electromagnetics and include magnetic inverse problems, integral equation methods, surface impedance boundary conditions, electromagnetic modeling of submarine and underground cables, and uncertainty quantification. He is a member of the Editorial Board of *COMPEL-The International Journal for Computation and Mathematics in Electrical and Electronic Engineering* and *Sensing and Imaging*. He is also an Associate Editor of *The Applied Computational Electromagnetics Society Journal* and IEEE Open Access Journal of Power and Energy.

MASSIMO BECHIS received the M.Sc. degree in nuclear engineering from Politecnico di Torino, in 1995. He joined Pirelli Cables (now Prysmian S.p.A.), in 1997. He is currently a System Innovation Manager with the Group Innovation Department. His working activity focuses on the development of multiphysics numerical models using FEM software with applications to heat transfer, fluid dynamics, applied electromagnetism, and structural analysis.

CARLO DE FALCO received the M.Sc. degree in electrical engineering from Politecnico di Milano, in 2002, and the Ph.D. degree in applied mathematics from Universitá Statale di Milano, in 2006. He held research and teaching positions at Bergische Universität Wuppertal and Dublin City University. Since 2009, he has been with Politecnico di Milano, where he is currently an Associate Professor of numerical analysis with the Modelling and Scientific Computing (MOX) Laboratory, Department of Mathematics. His research interests include numerical methods for solving partial differential equations with applications in electronics, electrical engineering, fluid dynamics, and material science.

Open Access funding provided by 'Politecnico di Milano' within the CRUI CARE Agreement